

# Dark matter distribution in dwarf spheroidal galaxies

Ewa L. Łokas

*Nicolaus Copernicus Astronomical Center, Bartycka 18, 00–716 Warsaw, Poland*

*E-mail: lokas@camk.edu.pl*

30 October 2018

## ABSTRACT

We study the distribution of dark matter in dwarf spheroidal galaxies by modelling the moments of their line-of-sight velocity distributions. We discuss different dark matter density profiles, both cuspy and possessing flat density cores. The predictions are made in the framework of standard dynamical theory of two-component (stars and dark matter) spherical systems with different velocity distributions. We compare the predicted velocity dispersion profiles to observations in the case of Fornax and Draco dwarfs. For isotropic models the dark haloes with cores are found to fit the data better than those with cusps. Anisotropic models are studied by fitting two parameters, dark mass and velocity anisotropy, to the data. In this case all profiles yield good fits but the steeper the cusp of the profile, the more tangential is the velocity distribution required to fit the data. To resolve this well-known degeneracy of density profile versus velocity anisotropy we obtain predictions for the kurtosis of the line-of-sight velocity distribution for models found to provide best fits to the velocity dispersion profiles. It turns out that profiles with cores typically yield higher values of kurtosis which decrease more steeply with distance than the cuspy profiles, which will allow to discriminate between the profiles once the kurtosis measurements become available. We also show that with present quality of the data the alternative explanation of velocity dispersions in terms of Modified Newtonian Dynamics cannot yet be ruled out.

**Key words:** methods: analytical – galaxies: dwarf – galaxies: fundamental parameters – galaxies: kinematics and dynamics – cosmology: dark matter

## 1 INTRODUCTION

Dark matter is now generally believed to be the dominating component of the matter content of the Universe which has played an important role in the formation of structure. Significant effort has gone into establishing its properties and mechanisms of evolution. The theoretical results which got most attention in the recent years concerned the shape of density profiles of dark matter haloes. Those were mainly obtained by the means of  $N$ -body simulations with the most popular being the so-called universal profile advocated by Navarro, Frenk and White (1997, hereafter NFW). NFW found (and others confirmed) that in a large range of masses the density profiles of cold dark matter haloes forming in various cosmologies can be fitted with a simple formula with only one fitting parameter. This density profile steepens from  $r^{-1}$  near the centre of the halo to  $r^{-3}$  at large distances. More recent simulations with higher resolution produce even steeper density profiles, with inner slopes  $r^{-3/2}$  (Fukushige & Makino 1997; Moore et al. 1998; see also Jing & Suto 2000).

Analytical calculations also predict density profiles with

steep inner cusps. The NFW profile is claimed to be reproduced in studies taking into account the merging mechanism (Lacey & Cole 1993) in the halo formation scenario (NFW, Avila-Reese, Firmani & Hernandez 1998). On the other hand, using an extension of the spherical infall model Łokas (2000) and Łokas & Hoffman (2000) have shown that if only radial motions are allowed the inner profiles have to be steeper than  $r^{-2}$  (in agreement with considerations based on distribution functions, see Richstone & Tremaine 1984). Although addition of angular momentum is known to make profiles shallower (White & Zaritsky 1992; Hiotelis 2002), its origin is not yet clear enough to make exact predictions.

The expected steep inner profiles are now being tested by comparison with observations of density profiles of galaxies and galaxy clusters. Some recent studies of clusters (e.g. van der Marel et al. 2000) claim good agreement between cluster observations and the NFW mass density profile, while other based on lensing find the dark matter to exhibit a smooth core (Tyson, Kochanski & dell’Antonio 1998, see also Williams, Navarro & Bartelmann 1999). In the case of galaxies, however, the situation is even more troubling. Flores & Primack (1994) and Moore (1994) were the first to

arXiv:astro-ph/0112023v2 27 Feb 2002

indicate that the NFW profile is incompatible with the rotation curves of spiral galaxies. More and more evidence is being presented now, which shows that spiral galaxies possess a dark matter core rather than a cusp in the inner parts (Burkert 1995; Salucci & Burkert 2000; Borriello & Salucci 2001). The evidence is especially convincing in the case of LSB galaxies which are supposed to be dominated by dark matter (de Blok et al. 2001; de Blok, McGaugh & Rubin 2001). Some mechanisms to explain the formation of such core have also been proposed (Hannestad 1999; Kaplinghat, Knox & Turner 2000; El-Zant, Shlosman & Hoffman 2001; Ravindranath, Ho & Filippenko 2001). However, as emphasized by van den Bosch & Swaters (2001) even good quality rotation curves cannot always discriminate between constant density cores and cusps because of the effects of beam smearing, the uncertainties in the stellar mass-to-light ratio and the limited spatial sampling of the halo density distribution.

Dwarf spheroidal (dSph) galaxies provide a unique testing tool for the presence and distribution of dark matter because due to their large velocity dispersions they are believed to be dominated by this component (for a review see Mateo 1997). Measurements of central velocity dispersion allowed many authors to estimate mass-to-light ratios in dwarfs and find it to be much larger than stellar values (see Mateo 1998a and references therein). These calculations were made with the simplifying assumption of isotropic velocity distribution and in most cases of mass following light. With the measured velocity dispersion profiles becoming available now, this assumption can in fact be relaxed and much more information can be extracted from the data. However, as in all pressure supported systems, when trying to model the velocity dispersion dependence on distance we are faced with the well-known degeneracy of density profile versus velocity anisotropy (Binney & Tremaine 1987).

The purpose of this work is to study moments of the line-of-sight velocity distribution following from different dark matter density profiles and different assumptions concerning velocity anisotropy. We focus on modelling the velocity dispersion profiles and extend here the earlier work (Lokas 2001), which discussed only NFW profile, by considering both cuspy profiles and those possessing flat cores, in order to decide which of them (and under what conditions) are favoured by observational data in the case of dSph galaxies. In order to discriminate between different models we also obtain predictions for the fourth-order velocity moment. Our work is complementary to the approach of Wilkinson et al. (2002) and Kleyna et al. (2001, 2002) who discussed dark matter distributions differing at large distances from the centre.

The paper is organized as follows. In Section 2 we briefly present the method of calculation of the line-of-sight velocity moments in models with different density profiles and velocity anisotropy. Section 3 describes the assumptions about the matter content of dSph galaxies. Results for the velocity dispersion profiles of Fornax and Draco dwarfs for both isotropic and anisotropic velocity distribution are given in Section 4, where we also present predictions for the fourth moment, the kurtosis. Section 5 provides comments on the possible alternative explanation of velocity dispersions in terms of Modified Newtonian Dynamics (MOND) and the discussion follows in Section 6.

## 2 MOMENTS OF THE VELOCITY DISTRIBUTION

The dynamics of stars in a gravitational potential  $\Phi(r)$  is completely described by the distribution function  $f(\mathbf{r}, \mathbf{v})$  governed by the Boltzmann equation. It is often advantageous however to work not with  $f$  but with its velocity moments defined as

$$\overline{\nu v_r^i v_\theta^j v_\phi^k} = \int v_r^i v_\theta^j v_\phi^k f(r, \mathbf{v}) d^3v, \quad (1)$$

where  $\nu(r)$  is a 3D density of stars. In the following we will assume that the system is spherically symmetric and that there are no net streaming motions (e.g. no rotation). Then all the odd velocity moments vanish.

At second order the two distinct moments are  $\overline{v_r^2}$  and  $\overline{v_\theta^2} = \overline{v_\phi^2}$  which we will denote hereafter by  $\sigma_r^2$  and  $\sigma_\theta^2$  respectively. They are related by the lowest order Jeans equation derived from the Boltzmann equation (Binney & Tremaine 1987)

$$\frac{d}{dr}(\nu\sigma_r^2) + \frac{2\beta}{r}\nu\sigma_r^2 + \nu\frac{d\Phi}{dr} = 0, \quad (2)$$

where

$$\beta = 1 - \frac{\sigma_\theta^2(r)}{\sigma_r^2(r)} \quad (3)$$

is a measure of the anisotropy in the velocity distribution and  $\Phi$  is the gravitational potential.

The most convenient approach to solving equation (2) for  $\sigma_r^2$  is to make an assumption about  $\beta$ . The values of this parameter have been studied both observationally and via  $N$ -body simulations but only in systems very different from dSph galaxies. For dark matter haloes Thomas et al. (1998) find that, in a variety of cosmological models, the ratio  $\sigma_\theta/\sigma_r$  is not far from unity and decreases slowly with distance from the centre to reach  $\simeq 0.8$  at the virial radius. Observations of elliptical galaxies are also consistent with the orbits being isotropic near the centre and somewhat radially anisotropic farther away, although cases with tangential anisotropy are also observed (Gerhard et al. 2001). In our considerations the anisotropy parameter describes the properties of the observed motion of stars which are only a tracer population of the underlying dark matter potential and therefore we cannot assume their anisotropy is similar to that of dark haloes or elliptical galaxies. In the absence of theory of their formation, which could provide some hints, or direct measurements of velocity anisotropy in dSph galaxies we have to consider different values of  $\beta$ .

Traditionally,  $\beta$  has been modelled in a way proposed by Osipkov (1979) and Merritt (1985) where  $\beta_{\text{OM}} = r^2/(r^2 + r_a^2)$ , with  $r_a$  being the anisotropy radius determining the transition from isotropic orbits inside to radial orbits outside. This model covers a wide range of possibilities from isotropy ( $r_a \rightarrow \infty, \beta = 0$ ) to radial orbits ( $r_a \rightarrow 0, \beta = 1$ ). Another possibility is that of tangential anisotropy with the fiducial case of circular orbits when  $\beta \rightarrow -\infty$ . For our purposes here it is most convenient to cover all possibilities from radial to isotropic and circular orbits with a simple model of  $\beta = \text{const}$  and  $-\infty < \beta \leq 1$ .

The solution of the Jeans equation (2) with the boundary condition  $\sigma_r \rightarrow 0$  at  $r \rightarrow \infty$  for  $\beta = \text{const}$  is

$$\nu\sigma_r^2(\beta = \text{const}) = r^{-2\beta} \int_r^\infty r^{2\beta} \nu \frac{d\Phi}{dr} dr. \quad (4)$$

From the observational point of view, an interesting, measurable quantity is the line-of-sight velocity dispersion obtained from the 3D velocity dispersion by integrating along the line of sight (Binney & Mamon 1982)

$$\sigma_{\text{los}}^2(R) = \frac{2}{I(R)} \int_R^\infty \left(1 - \beta \frac{R^2}{r^2}\right) \frac{\nu \sigma_r^2 r}{\sqrt{r^2 - R^2}} dr, \quad (5)$$

where  $I(R)$  is the surface brightness.

Introducing result (4) into equation (5) and inverting the order of integration the calculations of  $\sigma_{\text{los}}$  can be reduced to one-dimensional numerical integration of a formula involving special functions for arbitrary  $\beta = \text{const}$ .

It has been established that by studying  $\sigma_{\text{los}}(R)$  alone we cannot uniquely determine the properties of a stellar system. In fact systems with different densities and velocity anisotropies can produce identical  $\sigma_{\text{los}}(R)$  profiles (see e.g. Merrifield & Kent 1990; Merritt 1987). As will be shown below, the same kind of degeneracy also plagues the modelling of dSph galaxies. It is therefore interesting to consider higher-order moments of the velocity distribution hoping that the models with the same  $\sigma_{\text{los}}(R)$  will differ in their projected higher-order moments.

In the case of fourth-order moments we have three distinct components  $\overline{v_r^4}$ ,  $\overline{v_\theta^4} = \overline{v_\phi^4}$  and  $\overline{v_r^2 v_\theta^2} = \overline{v_r^2 v_\phi^2}$  related by two higher order Jeans equations (Merrifield & Kent 1990). In order to calculate the moments we need additional information about the distribution function. According to Jeans theorem the anisotropic distribution functions can be constructed as functions of the integrals of motion, the energy  $E = -\Phi - v^2/2$  and angular momentum  $L = (v_\theta^2 + v_\phi^2)^{1/2} r$ . In the isotropic case the distribution function is a function of energy alone and can be determined uniquely from the underlying mass distribution. However, as discussed by Dejonghe (1987), in the anisotropic case, in which we will be most interested here, the function is not uniquely determined by the assumed mass density, even if information on velocity dispersions is available.

Therefore we will restrict ourselves here to functions which can be constructed from the energy-dependent distribution function by multiplying it by some function of angular momentum. We will adopt the form

$$f(E, L) = f_0(E) L^{-2\beta} \quad (6)$$

with  $\beta = \text{const}$ , a generalization first considered by Hénon (1973). The velocity moments of such a function can be explored without explicit calculation of  $f_0(E)$ . For example, using equation (1) one can show that the function of the form (6) has the desired property of  $\sigma_\theta^2/\sigma_r^2 = 1 - \beta$ . Similar calculation proves that the three fourth-order moments are related by

$$\overline{v_r^2 v_\theta^2} = \frac{1}{3}(1 - \beta) \overline{v_r^4} \quad (7)$$

$$\overline{v_\theta^4} = \frac{1}{2}(1 - \beta)(2 - \beta) \overline{v_r^4}. \quad (8)$$

Then the two Jeans equations for the fourth-order moments reduce to one of the form

$$\frac{d}{dr}(\nu \overline{v_r^4}) + \frac{2\beta}{r} \nu \overline{v_r^4} + 3\nu \sigma_r^2 \frac{d\Phi}{dr} = 0, \quad (9)$$

similar to equation (2). The solution, in analogy to equation (4), is

$$\overline{\nu v_r^4}(\beta = \text{const}) = 3r^{-2\beta} \int_r^\infty r^{2\beta} \nu \sigma_r^2(r) \frac{d\Phi}{dr} dr. \quad (10)$$

By projection we obtain the line-of-sight fourth moment

$$\begin{aligned} \overline{v_{\text{los}}^4}(R) &= \frac{2}{I(R)} \int_R^\infty \left[ \left(1 - \frac{R^2}{r^2}\right)^2 + 2(1 - \beta) \right. \\ &\times \left. \frac{R^2(r^2 - R^2)}{r^4} + \frac{(2 - \beta)(1 - \beta) R^4}{2 r^4} \right] \frac{\nu \overline{v_r^4} r}{\sqrt{r^2 - R^2}} dr, \end{aligned} \quad (11)$$

where we used relations (7)-(8). Introducing equations (10) and (4) into (11) and inverting the order of integration the calculation of  $\overline{v_{\text{los}}^4}(R)$  can be reduced to two-dimensional numerical integration. A useful way to express the fourth projected moment is to scale it with  $\sigma_{\text{los}}^4$  in order to obtain the kurtosis

$$\kappa_{\text{los}}(R) = \frac{\overline{v_{\text{los}}^4}(R)}{\sigma_{\text{los}}^4(R)} \quad (12)$$

which will be discussed in Subsection 4.3.

### 3 MATTER CONTENT

We will now discuss different mass distributions contributed by stars and dark matter to the gravitational potential  $\Phi$  in equation (2).

#### 3.1 Stars

The distribution of stars is modelled in the same way as in Lokas (2001) i.e. by the Sérsic profile (Sérsic 1968, see also Ciotti 1991)

$$I(R) = I_0 \exp[-(R/R_S)^{1/m}], \quad (13)$$

where  $I_0$  is the central surface brightness and  $R_S$  is the characteristic projected radius of the Sérsic profile. The best-fitting Sérsic parameter  $m$  has been found to vary in the range  $1 \leq m \leq 10$  (Caon, Capaccioli & D'Onofrio 1993) for different elliptical galaxies, however for dSph systems  $m = 1$  is usually used, although in some cases other values of  $m$  are found to provide better fits (e.g. Caldwell 1999).

The 3D luminosity density  $\nu(r)$  is obtained from  $I(R)$  by deprojection

$$\nu(r) = -\frac{1}{\pi} \int_r^\infty \frac{dI}{dR} \frac{dR}{\sqrt{R^2 - r^2}}. \quad (14)$$

In the case of  $m = 1$  we get  $\nu(r, m = 1) = I_0 K_0(r/R_S)/(\pi R_S)$ , where  $K_0(x)$  is the modified Bessel function of the second kind. For other values of  $m$  in the range  $1/2 \leq m \leq 10$  an excellent approximation for  $\nu(r)$  is provided by (Lima Neto, Gerbal & Márquez 1999)

$$\nu(r) = \nu_0 \left(\frac{r}{R_S}\right)^{-p} \exp\left[-\left(\frac{r}{R_S}\right)^{1/m}\right] \quad (15)$$

$$\nu_0 = \frac{I_0 \Gamma(2m)}{2R_S \Gamma[(3-p)m]}$$

$$p = 1.0 - 0.6097/m + 0.05463/m^2.$$

The mass distribution of stars following from (15) is

$$M_*(r) = \Upsilon L_{\text{tot}} \frac{\gamma[(3-p)m, (r/R_S)^{1/m}]}{\Gamma[(3-p)m]}, \quad (16)$$

where  $\Upsilon = \text{const}$  is the mass-to-light ratio for stars,  $L_{\text{tot}}$  is the total luminosity of the galaxy and  $\gamma(\alpha, x) = \int_0^x e^{-t} t^{\alpha-1} dt$  is the incomplete gamma function.

### 3.2 Dark matter

We explore here different density distributions of dark matter which can be described by the following general formula

$$\rho(r) = \frac{\rho_{\text{char}}}{(r/r_s)^\alpha (1+r/r_s)^{3-\alpha}}, \quad (17)$$

where  $\rho_{\text{char}}$  is a constant characteristic density. As is immediately clear from equation (17), the inner slope of the profile is  $r^{-\alpha}$  while the outer one is always  $r^{-3}$ . We choose the parameter  $\alpha$  in the range  $0 \leq \alpha \leq 3/2$ , which covers a wide range of possible inner profiles. The cuspy profiles of  $\alpha > 0$  are motivated by the results of  $N$ -body simulations. The profile with  $\alpha = 1$  corresponds to the so-called universal profile proposed by NFW (see also Łokas & Mamon 2001) as a fit to the profiles of simulated haloes, while the profile with  $\alpha = 3/2$  is identical to the one following from higher resolution simulations of Moore et al. (1998). The profile with  $\alpha = 0$ , possessing an inner core is favoured by observations of spiral galaxies (see the Introduction) and is very similar (but not identical) to the profile proposed by Burkert (1995).

The scale radius  $r_s$  introduced in equation (17) marks the distance from the centre of the object where the slope of the profile is the average of the inner and outer slope:  $r^{-(3+\alpha)/2}$ . Additional parameter which controls the shape of the profile is the concentration which we define here in a traditional way as

$$c = \frac{r_v}{r_s}, \quad (18)$$

where  $r_v$  is the virial radius, i.e. the distance from the centre of the halo within which the mean density is  $v = 200$  times the present critical density,  $\rho_{\text{crit},0}$ . The density of  $200\rho_{\text{crit},0}$  is traditionally assumed by most  $N$ -body simulators to be the mean density of the object collapsing and virializing at the present epoch. This value, following from the spherical collapse model, depends however on the underlying cosmology, e.g.  $v = 178$  is valid for the Einstein-de Sitter model, while we have  $v \approx 100 - 120$  for the currently most popular  $\Lambda(\text{Q})\text{CDM}$  models with  $\Omega_M = 0.3$  and  $\Omega_{\Lambda(\text{Q})} = 0.7$  (Łokas & Hoffman 2001a, 2001b). However, since this study is motivated by the dark halo profiles obtained in  $N$ -body simulations we keep  $v = 200$  in order to have the same definition of concentration parameter as in most simulations.

We normalize the density profile (17) so that the mass within  $r_v$  is equal to the so-called virial mass

$$M_v = \frac{4}{3} \pi r_v^3 v \rho_{\text{crit},0}. \quad (19)$$

The characteristic density of equation (17) then becomes

$$\rho_{\text{char}} = \frac{(3-\alpha)v\rho_{\text{crit},0}c^\alpha}{3F(c)}, \quad (20)$$

where  $F(c)$  is given by the hypergeometric function

$$F(x) = {}_2F_1(3-\alpha, 3-\alpha; 4-\alpha; -x). \quad (21)$$

The dark mass distribution following from (17), (19) and (20) is

$$M_D(s) = M_v s^{3-\alpha} \frac{F(cs)}{F(c)}, \quad (22)$$

where we introduced  $s = r/r_v$ .

The concentration of simulated dark matter haloes has been observed to depend on the virial mass. Jing & Suto (2000) tested the relation  $c(M_v)$  for the masses of the order of normal galaxies and clusters in the case of density profiles with  $\alpha = 1$  and  $\alpha = 3/2$  and found the concentration to decrease with mass with the highest  $c \approx 10$  ( $\alpha = 1$ ) and  $c \approx 5$  ( $\alpha = 3/2$ ) observed for the mass scale of the order of a normal galaxy ( $10^{12} h^{-1} M_\odot$ ). In the previous work (Łokas 2001) we used an extrapolation of the  $c(M_v)$  relation fitted to the simulations results to smaller masses characteristic of dwarf galaxies. Here, however, similar relation would be needed for the  $\alpha = 0$  profile and the information provided by observations is very scarce. Although relations e.g. between the inner mass and core radius have been found in the case of Burkert profile (Burkert 1995) and those can be translated into an  $c(M_v)$  relation useful here, the estimates of this kind have been performed only for a small number of spiral galaxies and the errors of the fitted parameters are large (Borriello & Salucci 2001). We have therefore decided to assume different concentration parameters  $c = \text{const}$  in the further analysis. If we believe, however, that the trend of  $c$  decreasing with  $M_v$  extends to smaller masses (and the relation was found to be even steeper for subhalos by Bullock et al. 2001) we should expect the cuspy halos in dSph galaxies to have  $c > 10$  ( $\alpha = 1$ ) and  $c > 5$  ( $\alpha = 3/2$ ).

## 4 RESULTS FOR THE FORNAX AND DRACO DWARFS

In the two following subsections we model the velocity dispersion profile of Fornax and Draco first assuming isotropy and then for arbitrary anisotropy parameter  $\beta = \text{const}$ . In the third subsection we present predictions for the line-of-sight kurtosis for some of the best-fitting models.

### 4.1 Isotropic orbits

The observational parameters of the Fornax and Draco dwarfs needed in the following computation were taken from Irwin & Hatzidimitriou (1995) and are summarized in Table 1. The Table gives the fitted Sérsic radius  $R_S$  assuming the  $m = 1$  Sérsic distribution of equation (13), the distance modulus  $m - M$ , the distance in kpc with its error, the brightness of the galaxies in V-band,  $M_V$ , and the total luminosity in V-band,  $L_{\text{tot},V}$ , together with its error. We adopt the mass-to-light ratio for stars in this band to be  $\Upsilon_V \approx 1 M_\odot / L_\odot$  (Mateo et al. 1991).

In the previous work (Łokas 2001) it was shown that the density of stars alone cannot produce the observed velocity dispersion profiles in the case of Fornax and Draco. In the following we will explore the hypothesis that the velocity dispersions are generated by stars moving in the Newtonian gravitational acceleration generated by stars and dark matter.

We first assume that the velocity distribution of stars

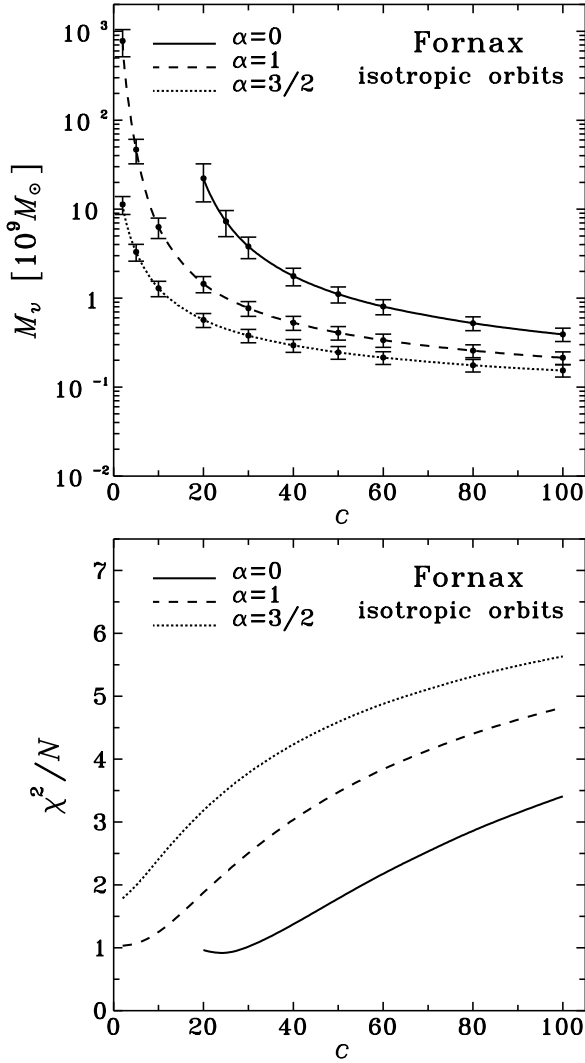


**Figure 1.** Upper panel: the best fitting masses of dark haloes as a function of assumed concentration parameter for profiles with different  $\alpha$  in the case of isotropic orbits for the Fornax dwarf. Lower panel: the goodness of fit measure,  $\chi^2/N$ , for the fits in the upper panel.

**Table 1.** Observational parameters of the Fornax and Draco dwarfs from Irwin & Hatzidimitriou (1995).

parameter	Fornax	Draco
$R_S$ (arcmin)	9.9	4.5
$R_S$ (kpc)	0.35	0.094
$m - M$	20.4	19.3
distance (kpc)	$120 \pm 8$	$72 \pm 3$
$M_V$ (mag)	-13.0	-8.3
$L_{\text{tot},V}(L_\odot)$	$(1.4 \pm 0.4) \times 10^7$	$(1.8 \pm 0.8) \times 10^5$

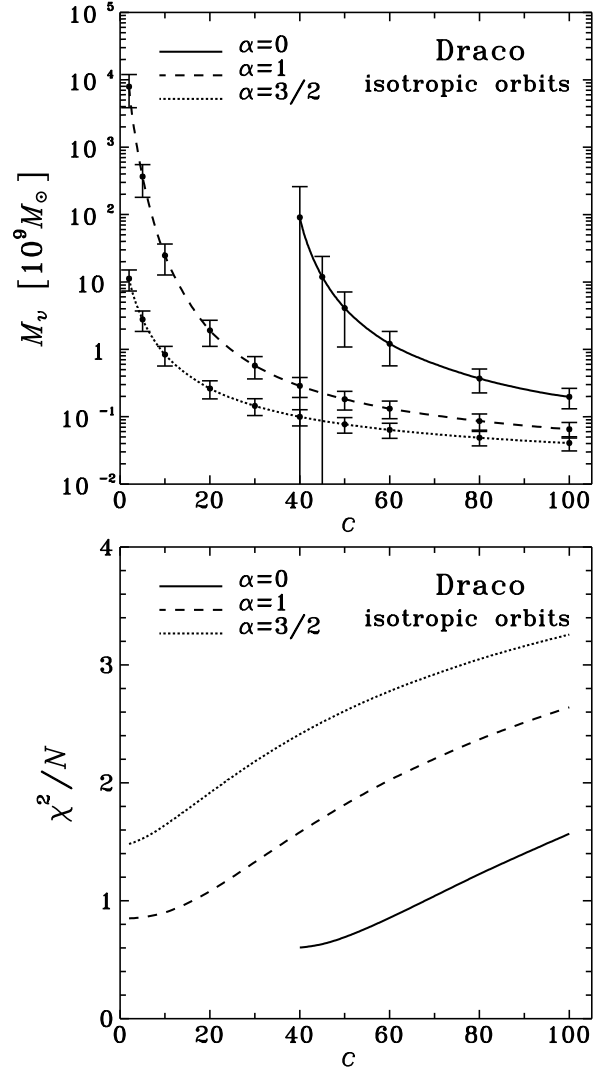


**Figure 2.** Same as Figure 1, but for Draco.

is isotropic, i.e. we consider models obtained from equations (4) and (5) in the case of  $\beta = 0$ . The 3D distribution of stars  $\nu(r)$  is given by (15). The gravitational acceleration is  $g = -d\Phi/dr = -GM(r)/r^2$  with  $M(r) = M_*(r) + M_D(r)$ , where  $M_*(r)$  and  $M_D(r)$  are given by equations (16) and (22), respectively. Using such modelling of the velocity dispersion profile we perform a one-parameter fitting of the velocity dispersion data. In the case of Fornax we use the data of Mateo (1997) and in the case of Draco those of Armandroff, Pryor & Olszewski 1997 (based on the observations of Armandroff, Olszewski & Pryor 1995). In each case we assume the value of the concentration parameter  $c$  and fit by the method of least squares (Brandt 1999) the dark virial mass  $M_v$  of the models with different dark matter profiles distinguished by the parameter  $\alpha$  of equations (17) and (22).

The resulting best-fitting values of  $M_v$  as a function of assumed  $c$  are shown in the upper panels of Figures 1 and 2. The error bars indicate  $1\sigma$  errors in  $M_v$  associated with the errors in the velocity dispersion measurements. They

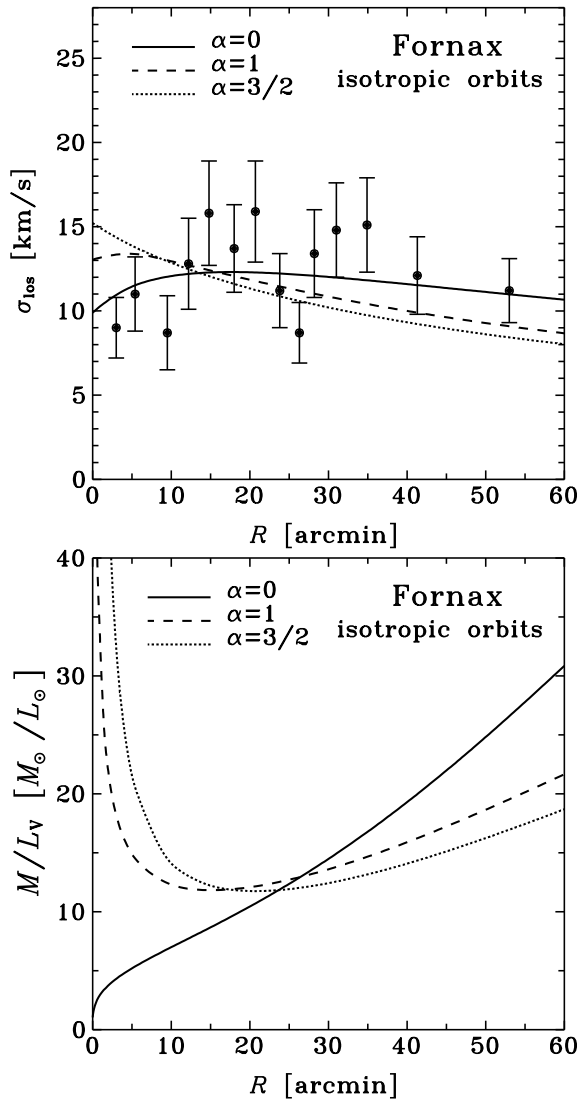


**Figure 3.** Upper panel: the best fitting velocity dispersion profiles obtained for  $c = 30$  ( $\alpha = 0$ ),  $c = 20$  ( $\alpha = 1$ ) and  $c = 10$  ( $\alpha = 3/2$ ) in the case of isotropic orbits for the Fornax dwarf. Lower panel: mass-to-light ratios for the fits in the upper panel.

are obtained from the covariance matrix (in this case one-element) of the fitted parameters. The errors in mass in the whole range of concentrations shown in Figures 1 and 2 are of the order of 16-45% for Fornax and 24-185% for Draco. The lower panels of these Figures plot  $\chi^2/N$ , the measure of the goodness of fits presented in the upper panels, where  $N$  is the number of degrees of freedom (in this case we have  $N = 13$  for Fornax and  $N = 4$  for Draco). The results for  $\alpha = 0$  do not reach to very low concentration because the least-square fitting converges more and more slowly there yielding incredibly high dark masses. One might think that a two-parameter ( $c, M_v$ ) fitting would be a better choice here, but as the lower panels of Figures 1 and 2 show, this would give the lowest possible  $c$  in all cases. In the case of cuspy profiles resulting from  $N$ -body simulations low  $c$  of the order of unity is never obtained except for objects of the mass of cluster of galaxies. Clearly for both Fornax and Draco

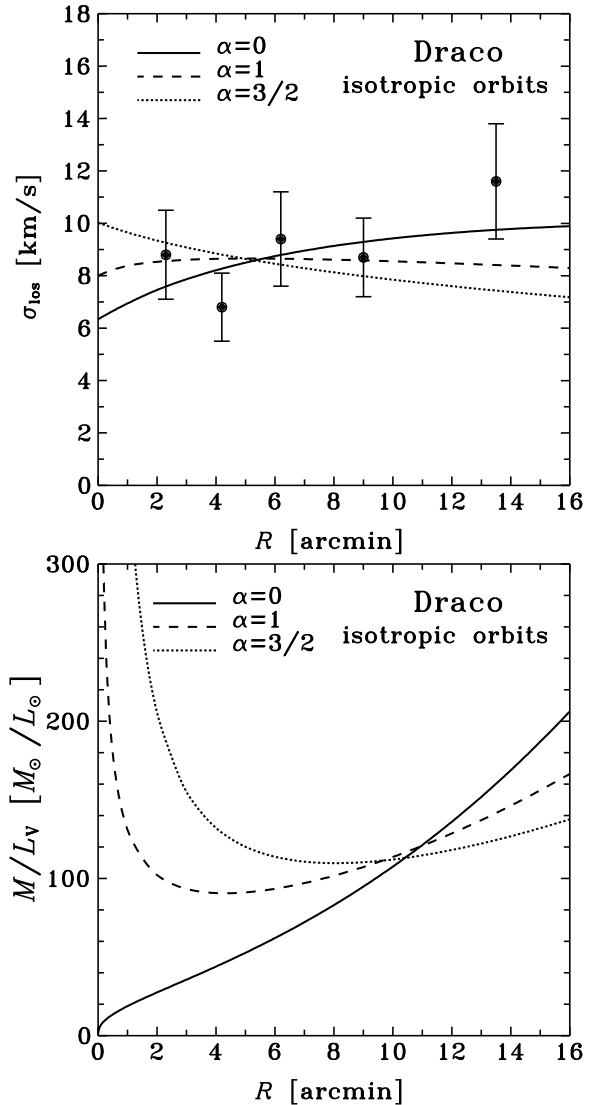


**Figure 4.** Same as Figure 3, but for Draco. The best fitting velocity dispersion profiles plotted were obtained for  $c = 50$  ( $\alpha = 0$ ),  $c = 20$  ( $\alpha = 1$ ) and  $c = 10$  ( $\alpha = 3/2$ ).

the  $\alpha = 0$  profile provides the best fit in terms of  $\chi^2/N$ . Although quite low  $\chi^2/N$  can be also obtained for  $\alpha = 1$  profile, this happens only for unrealistic low concentrations and yielding incredibly high mass of a halo of the order of a normal galaxy.

The predictions for the line-of-sight velocity dispersion profiles of the best-fitting models with  $\alpha = 0, 1$  and  $3/2$  in the isotropic case are shown in the upper panels of Figures 3 and 4 for Fornax and Draco respectively together with the data. For clarity of the illustration we have chosen only one of the fits from Figures 1 and 2 for each type of profile. In the case of  $\alpha = 0$  profile no a priori information on  $c$  is available so we have chosen the value giving the best fit and reasonably low best-fitting mass  $M_v$  at the same time, i.e.  $c = 30$  in the case of Fornax and  $c = 50$  in the case of Draco. For cuspy profiles the concentrations expected on the basis of the  $N$ -body results were chosen (see Subsection 3.2). We

**Table 2.** Examples of best-fitting parameters in the isotropic and anisotropic case with  $1\sigma$  error bars.  $M_v$  is given in units of  $10^9 M_\odot$ .

case	$\alpha$	parameter	Fornax	Draco
$\beta = 0$	0	$M_v$	$3.8 \pm 1.0(1.2)$	$4.1 \pm 3.0(3.2)$
	1	$M_v$	$1.5 \pm 0.3(0.3)$	$1.9 \pm 0.8(0.8)$
	3/2	$M_v$	$1.3 \pm 0.3(0.3)$	$0.84 \pm 0.27(0.27)$
$\beta \neq 0$	0	$M_v$	$3.4 \pm 1.0(1.1)$	$4.3 \pm 3.4(3.6)$
		$\beta$	$-0.36 \pm 0.33$	$-0.11 \pm 0.47$
	1	$M_v$	$1.3 \pm 0.3(0.3)$	$2.4 \pm 1.1(1.2)$
		$\beta$	$-1.5 \pm 0.8$	$-0.98 \pm 1.2$
	3/2	$M_v$	$1.2 \pm 0.3(0.3)$	$1.2 \pm 0.4(0.4)$
		$\beta$	$-2.6 \pm 1.6$	$-3.5 \pm 5.1$

have taken  $c = 20$  for  $\alpha = 1$  and  $c = 10$  for  $\alpha = 3/2$ . The best-fitting virial masses obtained for these concentrations in the isotropic case together with  $1\sigma$  error bars following from the uncertainties in velocity dispersion measurements are given in the upper part of Table 2. The method of least squares applied here allows also to study the propagation of errors associated with other observables entering the models. Including the errors in luminosity and distance given in Table 1 and assuming an error in the stellar mass-to-light ratio of  $0.5M_\odot/L_\odot$  (an estimate given by Mateo et al. (1991) in the case of Fornax) we obtain errors for  $M_v$  which are given in brackets in Table 2.

Lower panels of Figures 3 and 4 show the combined mass-to-light ratio in V-band for Fornax and Draco calculated from

$$M/L_V = \frac{M_D(r) + M_*(r)}{L_V(r)}, \quad (23)$$

where  $M_D(r)$  and  $M_*(r)$  are given by equations (22) and (16) respectively, and  $L_V(r) = M_*(r)/Y_V$  is the luminosity distribution. Calculation of  $M/L_V$  were made for the same models as presented in the upper panels of the Figures. The growth of  $M/L_V$  at large distances is due to the behaviour of  $M_D(r)$  which diverges logarithmically for all considered  $\alpha$  while the mass in stars is finite. However, while the cuspy profiles produce divergent  $M/L_V$  at the centre of the galaxy, the  $\alpha = 0$  profile gives a finite  $M/L_V$  increasing at all radii.

All the mass-to-light estimates shown give a similar  $M/L_V \approx 10M_\odot/L_\odot$  in the case of Fornax and  $M/L_V \approx 100M_\odot/L_\odot$  in the case of Draco at a scale of the order of two Sérsic radii and are consistent with the values of the central mass-to-light ratios given by Mateo et al. (1991) and Armandroff et al. (1997).

Kleyna et al. (2001) estimated mass-to-light ratio for Draco using their new velocity measurements (Kleyna et al. 2002). Assuming isotropic orbits and the velocity dispersion to be constant or a linear function of distance they calculated the mass needed to produce such velocities from the Jeans equation. The resulting  $M/L_V$  at three core radii (30 arcmin) turned out to be in the range of 350-1000. For this distance our isotropic models give  $M/L_V = 593, 369$  and  $250$  for  $\alpha = 0, 1$  and  $3/2$  respectively.

## 4.2 Anisotropic orbits

Comparing the predictions shown in upper panels of Figures 3 and 4 with the data we find that the cuspy profiles have to be aided by a certain amount of tangential anisotropy in order to better reproduce the shape of the observed velocity dispersion profiles. Trying more radial anisotropy than in the case of isotropic orbits by using positive values of  $\beta$  makes the curves decrease even more steeply with distance, contrary to the trend observed in the data. In the case of the profile with  $\alpha = 0$  it is not clear whether more radial or more tangential anisotropy would provide a better fit. Therefore in what follows we perform a two-parameter fitting of the velocity dispersion profiles with velocity anisotropy  $\beta = \text{const}$  as a second free parameter in addition to the dark mass,  $M_v$ .

The results of such least squares fitting procedure of the Fornax and Draco data are shown in Figures 5 and 6. The Figures are analogous to Figures 1 and 2 for the isotropic case except for the added uppermost panels showing the best-fitting  $\beta$  parameters with their  $1\sigma$  error bars. The estimated dark virial masses in the middle panels are now roughly the same for Fornax and somewhat higher for Draco than for isotropic orbits while their errors are now 17-50% for Fornax and 31-105% for Draco for the whole range of concentrations. The quality of fits (bottom panels) in terms of  $\chi^2/N$  (here  $N = 12$  for Fornax and  $N = 3$  for Draco) is now significantly better for cuspy profiles and also somewhat improved for the profiles with  $\alpha = 0$ . However, the profiles with cores produce best-fitting  $\beta$  closest to zero.

Figures 7 and 8 are the anisotropic analogues of Figures 3 and 4. As in the isotropic case for  $\alpha = 0$  profile we have chosen  $c = 30$  in the case of Fornax and  $c = 50$  in the case of Draco, while for cuspy profiles we have taken  $c = 20$  for  $\alpha = 1$  and  $c = 10$  for  $\alpha = 3/2$ . These values of concentrations happen to be those where  $\chi^2/N$  reaches minimum for different profiles in the case of Fornax (see the lowest panel of Figure 5). Upper panels of Figures 7 and 8 prove that when arbitrary anisotropy parameters are allowed acceptable fits can be obtained with all profiles. However, cuspy profiles require significantly more tangential anisotropy, i.e. lower  $\beta$  than the profile possessing a core.

The best-fitting values of  $M_v$  and  $\beta$  used in Figures 7 and 8 are given in the lower part of Table 2 together with their errors following from the uncertainties in velocity dispersion measurements. As in the isotropic case the errors in brackets for  $M_v$  include the effect of uncertainties in luminosity, distance and stellar mass-to-light ratio. The error estimates of  $\beta$  are not significantly affected by these additional factors and are not listed. It is clear from Table 2 that in all cases the measurements of velocity dispersion are the dominant source of error, while other sources affect the results only slightly and more for dark matter profiles with lower  $\alpha$ . One may object, however, that the distance errors given in Table 1 are rather small and do not encompass higher distance estimates by other authors (Mateo 1998b). Increasing the adopted distances by 10 kpc would decrease the virial masses given in Table 2 by up to 10% for Fornax and 40% for Draco for  $\alpha = 0$  with almost no difference for  $\alpha = 3/2$  (the estimates of  $\beta$  would remain roughly the same).

One may also wonder how the best-fitting parameters

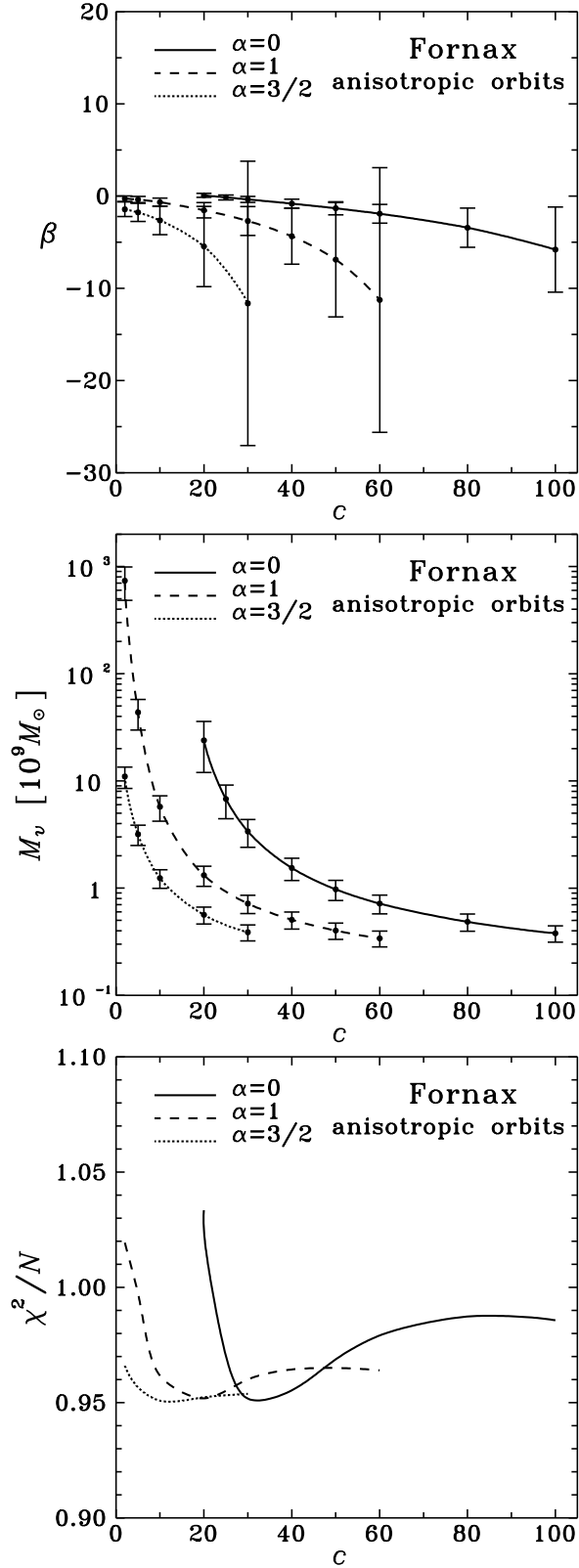


**Figure 5.** The best fitting anisotropy parameters  $\beta$  (upper panel) and masses of dark haloes (middle panel) as a function of assumed concentration parameter for profiles with different  $\alpha$  in the case of anisotropic orbits for the Fornax dwarf. Lower panel: the goodness of fit measure,  $\chi^2$ , for the fits in the upper panels.

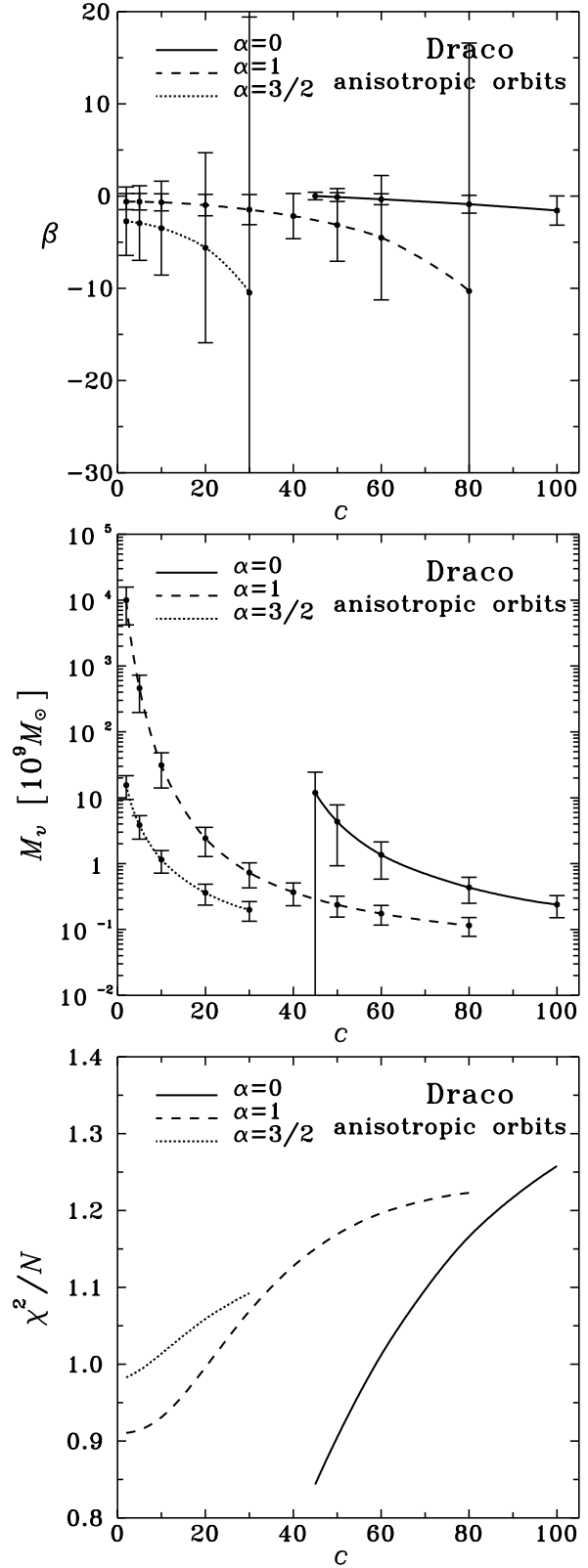


**Figure 6.** Same as Figure 5, but for Draco.



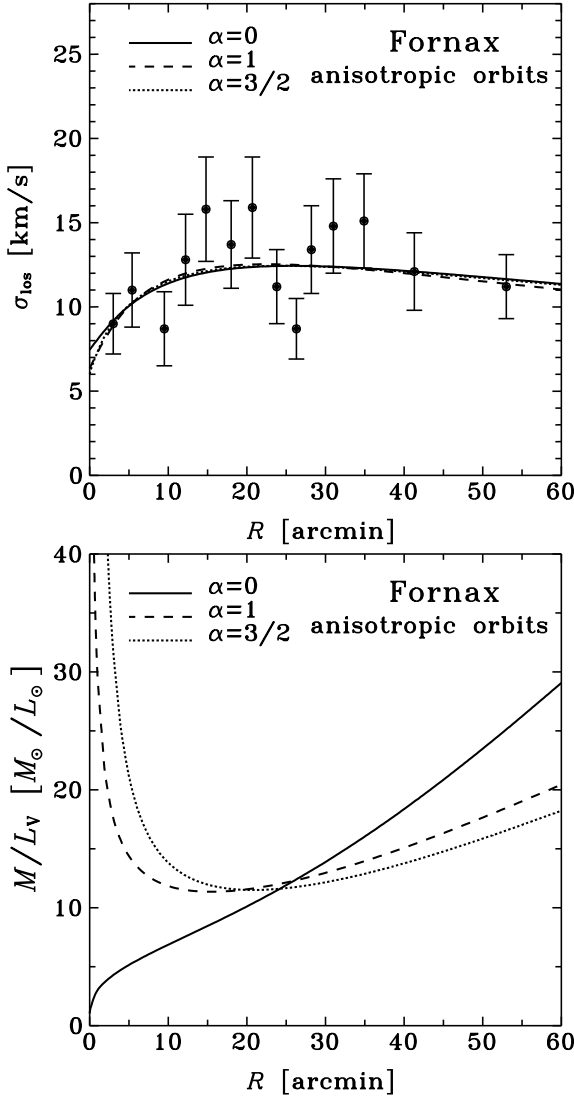


**Figure 7.** Upper panel: the best fitting velocity dispersion profiles obtained for  $c = 30$  ( $\alpha = 0$ ),  $c = 20$  ( $\alpha = 1$ ) and  $c = 10$  ( $\alpha = 3/2$ ) in the case of anisotropic orbits for the Fornax dwarf. Lower panel: mass-to-light ratios for the fits in the upper panel.

are affected by our definition of the virial mass. It turns out that decreasing the parameter  $v$  in equation (19) by a factor of two changes mainly best-fitting  $M_v$  (leaving  $\beta$  roughly the same) for the same value of concentration by increasing it typically by a factor of a few, more for lower  $\alpha$  and lower  $c$  (it must be emphasized however, that  $c$  given by equation (18) would then be a different quantity since  $r_v$  for a given  $M_v$  would be increased).

The mass-to-light ratios shown in the lower panels of Figures 7 and 8 do not change significantly with respect to the isotropic case and the very different behaviour for cuspy profiles versus the profile with a core is preserved. In the case of Draco at  $R = 30$  arcmin our anisotropic models give  $M/L_V = 606, 414$  and  $300$  for  $\alpha = 0, 1$  and  $3/2$  respectively, values slightly higher than in the isotropic case. The values agree to the order of magnitude with the estimate given by

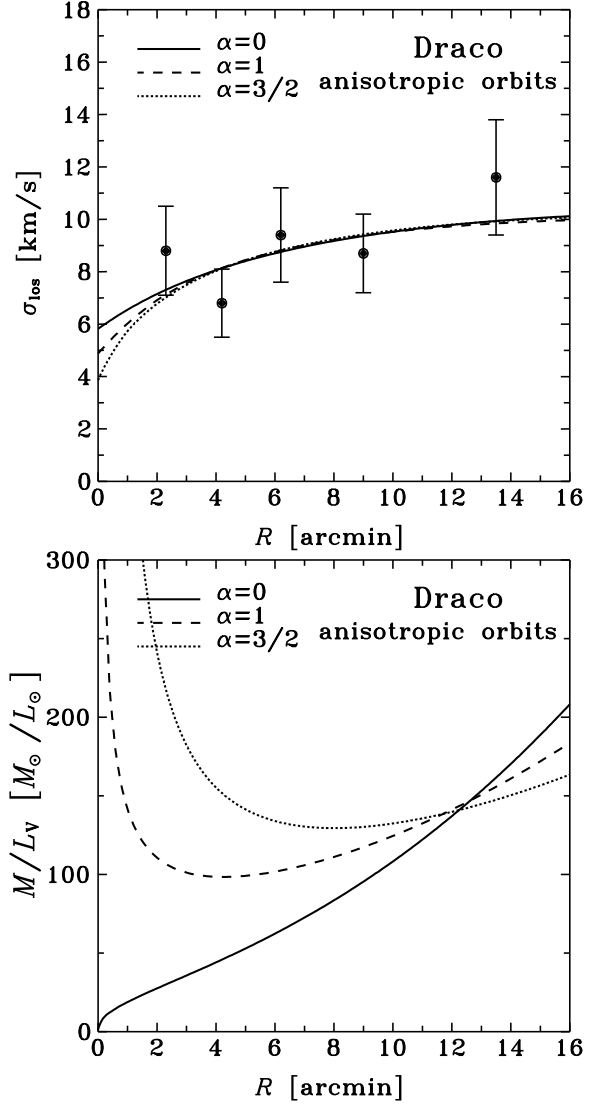


**Figure 8.** Same as Figure 7, but for Draco. The best fitting velocity dispersion profiles plotted were obtained for  $c = 50$  ( $\alpha = 0$ ),  $c = 20$  ( $\alpha = 1$ ) and  $c = 10$  ( $\alpha = 3/2$ ).

Kleyna et al. (2002) who find mass-to-light ratio of 330 for their best-fitting anisotropic model of Draco.

### 4.3 Predictions for the kurtosis

In the previous subsection we have shown that when velocity anisotropy is treated as a free parameter equally good fits to velocity dispersion profiles can be obtained with both cuspy profiles and the profile with a core. In order to get rid of this degeneracy and discriminate between the profiles one has to resort to higher order moments of the velocity distribution such as the kurtosis introduced in Section 2. Figure 9 shows the predictions for this quantity for models which turned out to provide best fits to velocity dispersion profiles of Fornax and Draco. The parameters used for every type of profile were taken from Table 2. In each panel the thick lines show

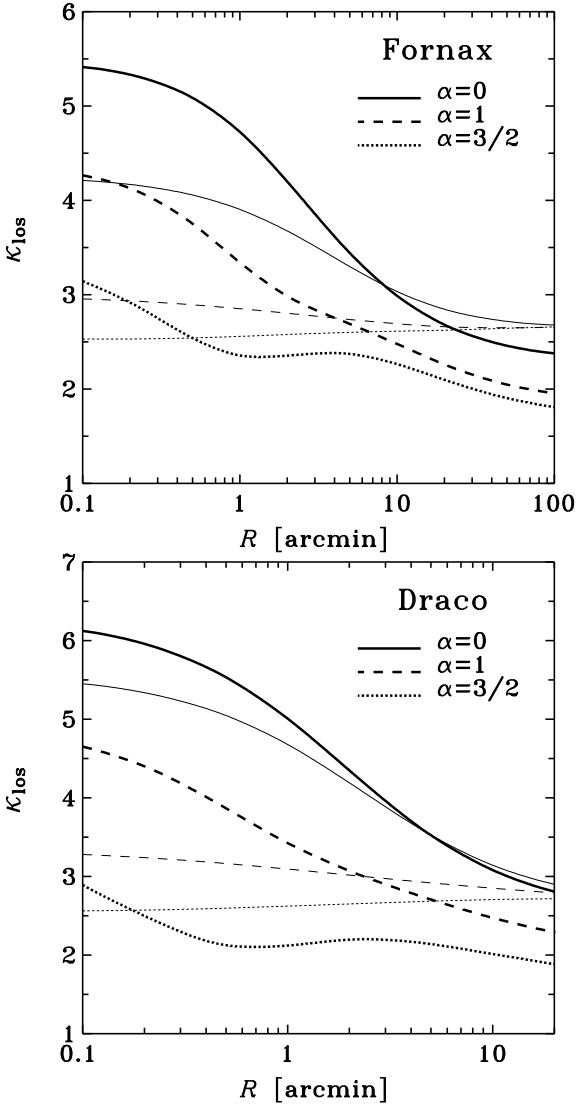


**Figure 9.** Kurtosis predictions for the best fitting models of Table 2 for Fornax (upper panel) and Draco (lower panel). Thick lines show the results for anisotropic models while thin lines for isotropic ones.

the predictions for anisotropic models while thin lines for isotropic ones.

The results prove that the kurtosis can indeed differentiate between the profiles with a cusp and those with a core. In the anisotropic case we find for both galaxies that the profile with a core results in a higher value of the kurtosis at a given distance from the centre and its value decreases more steeply with  $R$  than in the case of cuspy profiles. The situation is similar in the case of isotropic orbits, but here  $\kappa_{\text{los}}(R)$  definitely decreases with distance only for the  $\alpha = 0$  profile while its values remain almost constant for the cuspy profiles (slightly decreasing for  $\alpha = 1$  and slightly increasing for  $\alpha = 3/2$ ).

**Table 3.** Best-fitting parameters for MOND in the isotropic and anisotropic case with  $1\sigma$  error bars.  $a_0$  is given in units of  $10^{-8}\text{cm/s}^2$ , while  $M/L_V$  in  $M_\odot/L_\odot$ .

case	assumed	fitted	Fornax	Draco
$\beta = 0$	$M/L_V = 1$	$a_0$	$2.2 \pm 0.5(0.8)$	$39 \pm 13(22)$
	$a_0 = 1.2$	$M/L_V$	$1.8 \pm 0.4(0.7)$	$32 \pm 10(18)$
$\beta \neq 0$	$M/L_V = 1$	$a_0$	$2.1 \pm 0.5(0.8)$	$50 \pm 19(29)$
		$\beta$	$-0.96 \pm 0.53$	$-1.5 \pm 1.6$
	$a_0 = 1.2$	$M/L_V$	$1.8 \pm 0.4(0.7)$	$40 \pm 14(23)$
		$\beta$	$-0.97 \pm 0.53$	$-1.5 \pm 1.7$

## 5 ALTERNATIVE: MOND

DSph galaxies have low densities and therefore they lie in the regime of small accelerations. According to Modified Newtonian Dynamics (MOND), the theory proposed by Milgrom (1983), for accelerations below the characteristic scale of  $a_0 \approx 10^{-8}\text{cm/s}^2$  the laws of Newtonian dynamics may change affecting either inertia or gravity and mimic the presence of dark matter. Although originally designed to explain flat rotation curves of spiral galaxies, MOND is expected to operate in all low-acceleration systems. It has been e.g. shown to explain many observed features of LSB galaxies by McGaugh & de Blok 1998. On the other hand, Lake (1989) claimed MOND to be inconsistent with rotation curves of a few dwarf galaxies (the required values of  $a_0$  being different for different systems and generally too low). In the case of dSph galaxies MOND should cause an increase of velocity dispersions.

It is presently far from clear, whether MOND can explain the observed velocity dispersions of dSph galaxies. Although for most dwarfs it gives satisfactory results, notorious problems have been caused by Draco. Analyzing its central velocity dispersion Gerhard & Spergel (1992) have found it incompatible with stellar mass-to-light ratios, contrary to the conclusion of Milgrom (1995) who claimed that its mass-to-light ratio is consistent with stellar values if all the observational errors are properly taken into account.

In the previous work (Łokas 2001) we have shown how to generalize the method of predicting the line-of-sight velocity dispersion profile to MOND and applied it to fit the data for Fornax, Draco and Ursa Minor dwarfs. We have assumed the stellar mass-to-light ratio of  $M/L_V = 1M_\odot/L_\odot$  and fitted parameters  $a_0$  and  $\beta$ . The best-fitting values of  $a_0$  were different for different dwarfs, acceptable for Fornax, but much higher than expected in the case of Draco and Ursa Minor. We concluded that while the case of Ursa is doubtful since it has been recently observed to possess tidal tails (Martínez-Delgado et al. 2001), the high value of  $a_0$  estimated for Draco can pose a serious problem for MOND (a similar conclusion based on the analysis of a velocity dispersion profile of Draco from a different data set was also recently reached by Kley et al. 2001).

We have repeated the analysis here for Fornax and Draco with the least-square fitting method, similar to that applied to fit dark matter profiles, in order to provide the error estimates for the fitted parameters. Both isotropic and anisotropic cases were studied. The results of the fitting procedure are shown in Table 3 with the isotropic case in the

upper part and the anisotropic in the lower. We assumed  $M/L_V = 1M_\odot/L_\odot$  and fitted the acceleration parameter  $a_0$  in one case while taking  $a_0 = 1.2 \times 10^{-8} \text{ cm/s}^2$ , the value known to fit best the rotation curves of spiral galaxies (Begegan, Broeils & Sanders 1991; Sanders & Verheijen 1998), and finding  $M/L_V$  in the other.

As is clear from Table 3 both approaches yield acceptable values of  $M/L_V$  or  $a_0$  in the case of Fornax, while very high numbers in the case of Draco. However, the errors for Draco estimated from the uncertainties in the velocity dispersion measurements are so large that the acceptable values of  $M/L_V$  or  $a_0$  (of the order of unity in the units of the Table) are still within  $3\sigma$  error bars. Analysis of the velocity dispersion profile therefore reduces the error significantly compared to what can be obtained from a single central velocity dispersion measurement (then acceptable  $M/L_V$  are within  $2\sigma$  error from the best-fitting value, McGaugh, private communication), but still not enough to rule out MOND. In fact these errors are farther increased if the errors in luminosity measurement (quite big in the case of Draco, see Table 1) and in distance are taken into account. The resulting larger errors (due mainly to the error in luminosity) are given in brackets in Table 3. With these errors the values obtained here are safely within  $2\sigma$  of the acceptable ones. (A discussed in Section 4 this source of error is not important for dark matter because it dominates strongly the distribution of stars.) We therefore conclude that with present quality of the data the alternative explanation of velocity dispersions in terms of MOND cannot yet be ruled out.

## 6 DISCUSSION

We presented predictions for the line-of-sight velocity dispersion profiles of dwarf spheroidal galaxies and compared them to observations in the case of the Fornax and Draco dwarfs. We discussed different dark matter distributions, both cuspy and possessing flat density cores. For isotropic models the dark haloes with cores are found to generally fit the data better than those with cusps. The fits for each type of profile tend to be better for lower concentrations. For cuspy profiles those cannot be taken arbitrarily low since, as discussed in Subsection 3.2,  $N$ -body simulations (providing the basis for the choice of profiles here) predict higher concentrations for smaller masses. Besides, fits with low concentration require incredibly high corresponding dark masses of the order of a normal galaxy. In our exemplary cases we have taken  $c = 10$  for  $\alpha = 3/2$  and  $c = 20$  for  $\alpha = 1$ . The dark matter profiles with such parameters yield for Draco fits with  $\chi^2/N = 1.6$  and  $\chi^2/N = 1$ , respectively, while an  $\alpha = 0$  profile with  $c = 50$  has  $\chi^2/N = 0.6$ . The situation is similar for Fornax.

Anisotropic models were studied by fitting two parameters, dark mass and velocity anisotropy, to the data. We find that the steeper the cusp of the profile, the more tangential is the velocity distribution required to fit the data, in agreement with the well-known degeneracy of density profile versus velocity anisotropy. In this case acceptable fits (with  $\chi^2/N = 1$  or lower) can be obtained for all considered profiles, but only the profiles with cores yield good fits with anisotropy parameter close to the isotropic value. To discriminate between different profiles we offer predictions for

the kurtosis of the line-of-sight velocity distribution. Our findings in the case of the velocity dispersion profile for Draco are complementary to and in qualitative agreement with those of Kleyna et al. (2002) who tested dark matter distributions varying at large distances. Their best-fitting models required the halo to be nearly isothermal (as our models are in a wide range of distances) and the velocity anisotropy to be weakly tangential.

The amount of dark matter inferred depends on the concentration parameter of the density profile, but for realistic concentrations is typically of the order of  $10^9 M_\odot$  both for Fornax and Draco for all profiles and velocity distributions. Since the total luminosity of Draco is two orders of magnitude lower than that of Fornax (see Table 1), this results in a significant difference in their corresponding mass-to-light ratios. At the scale of the order of two Sérsic radii Fornax has  $M/L_V \approx 10M_\odot/L_\odot$  while for Draco we obtain  $M/L_V \approx 100M_\odot/L_\odot$ . However, mass-to-light ratio dependence on distance is very different for different profiles. For cuspy profiles  $M/L_V$  diverges both at small and at large distances from the centre, while for  $\alpha = 0$  profile it is finite at the centre and grows steadily with distance. For distances larger than two Sérsic radii profiles with lower  $\alpha$  give higher values of  $M/L_V$  and the anisotropic models yield slightly higher  $M/L_V$  than isotropic ones. As discussed in Section 3, our results for  $M/L_V$  outside the galactic core agree to the order of magnitude with the estimates of Kleyna et al. (2001, 2002).

A possible source of uncertainty in the analysis of velocity dispersions is the influence of binary population. In the recent study De Rijcke & Dejonghe (2002) using realistic distributions of orbital parameters estimated the maximum additional velocity dispersion due to binary stars to be of the order of 3 km/s (in agreement with earlier studies). It turns out that only stellar systems with intrinsic dispersions close to this value (e.g. globular clusters) will be affected. For velocity dispersions characteristic of dSph galaxies studied here the effect is small: the velocity dispersion  $\sigma = 9$  km/s for a galaxy with a Gaussian line-of-sight velocity distribution can increase due to the presence of binaries by at most 5% (for the maximum binary fraction of 1, see Figure 15 of De Rijcke & Dejonghe 2002), much less than the typical error in velocity dispersion measurements. The binary fraction of Draco is estimated to be between 0.2 (Olszewski, Pryor & Armandroff 1996) and 0.4 (Kleyna et al. 2002), which would make the effect even smaller. For Fornax no information on binaries is yet available, but the typical velocity dispersions are higher in this galaxy which makes the effect less important. We therefore expect binaries to only slightly affect our best-fitting models so as to increase the estimated virial mass. More influence is expected in the case of kurtosis: its Gaussian value  $\kappa_{\text{los}} = 3$  for the same dispersion  $\sigma = 9$  km/s will increase by up to 23%. Hence when using the kurtosis predictions of Subsection 4.3 to discriminate between different dark matter profiles the influence of binary population will have to be studied in more detail.

The analysis presented in this paper is valid under the condition that dSph galaxies are in dynamical equilibrium. However, those of them studied here, as members of the Local Group exist in gravitational field of larger galaxy, the Milky Way. One may worry that the tidal interactions with bigger galaxy may affect the dynamics of some dwarfs

and our interpretations of their velocity dispersions. Some of the dwarfs have been indeed observed to possess tidal tails, e.g. Ursa Minor (Martínez-Delgado et al. 2001), Sagittarius (Ibata, Gilmore & Irwin 1994) or Carina (Majewski et al. 2000). However, in the case of Draco dwarf studied here no evidence of tidal interactions was found (Piatek et al. 2002).

Tidal interactions have been studied theoretically by numerical modelling with conflicting results. Piatek & Pryor (1995) have performed numerical simulations of such effects and concluded that they should not affect much the inferred mass-to-light ratios. However, Kroupa (1997) and Klessen & Kroupa (1998) have demonstrated that what appears to be a dSph galaxy in equilibrium may in fact be a tidal remnant displaying high velocity dispersions without any dark matter. As suggested by Oh, Lin & Aarseth (1995) it may also very well be that some dwarfs indeed contain dark matter while others may be part of tidal debris. It is still debated, whether tidal interactions are common among dSph galaxies and whether they may cause an increase of velocity dispersion that is likely to be interpreted as presence of dark matter.

## ACKNOWLEDGEMENTS

I wish to thank P. Salucci for encouragement to follow the line of investigation presented in this paper and S. McGaugh for discussions on dSph galaxies in MOND. Extensive comments from an anonymous referee helped to significantly improve the paper. This research was partially supported by the Polish State Committee for Scientific Research grant No. 2P03D02319.

## REFERENCES

- Armandroff T. E., Olszewski E. W., Pryor C., 1995, *AJ*, 110, 2131  
 Armandroff T. E., Pryor C., Olszewski E. W., 1997, in Sofue Y., ed., *Proc. IAU Symp. 184, The Central Regions of the Galaxy and Galaxies*. Kluwer, Dordrecht, p. 35  
 Avila-Reese V., Firmani C., Hernandez X., 1998, *ApJ*, 505, 37  
 Begeman K. G., Broeils A. H., Sanders R. H., 1991, *MNRAS*, 249, 523  
 Binney J., Mamon G. A., 1982, *MNRAS*, 200, 361  
 Binney J., Tremaine S., 1987, *Galactic Dynamics*. Princeton Univ. Press, Princeton, chap. 4.  
 Borriello A., Salucci P., 2001, *MNRAS*, 323, 285  
 Brandt S., 1999, *Data Analysis and Computational Methods for Scientists and Engineers*. Springer Verlag, New York, chap. 9  
 Bullock J. S., Kolatt T. S., Sigad Y., Somerville R. S., Kravtsov A. V., Klypin A. A., Primack J. R., Dekel A., 2001, *MNRAS*, 321, 559  
 Burkert A., 1995, *ApJ*, 447, L25  
 Caon N., Capaccioli M., D’Onofrio M., 1993, *MNRAS*, 265, 1013  
 Caldwell N., 1999, *AJ*, 118, 1230  
 Ciotti L., 1991, *A&A*, 249, 99  
 de Blok W. J. G., McGaugh S. S., Bosma A., Rubin V. C., 2001, *ApJ*, 552, L23  
 de Blok W. J. G., McGaugh S. S., Rubin V. C., 2001, *AJ*, 122, 2396  
 Dejonghe H., 1987, *MNRAS*, 224, 13  
 De Rijcke S., Dejonghe H., 2002, *MNRAS*, 329, 829  
 El-Zant A., Shlosman I., Hoffman Y., 2001, *ApJ*, 560, 636  
 Flores R. A., Primack J. R., 1994, *ApJ*, 427, L1  
 Fukushige T., Makino J., 1997, *ApJ*, 477, L9  
 Gerhard O. E., Spergel D. N., 1992, *ApJ*, 397, 38  
 Gerhard O., Kronawitter A., Saglia R. P., Bender R., 2001, *AJ*, 121, 1936  
 Hannestad S., 1999, *astro-ph/9912558*  
 Hénon M., 1973, *A&A*, 24, 229  
 Hioteles N., 2002, *A&A*, 382, 84  
 Ibata R. A., Gilmore G. & Irwin M. J., 1994, *Nature*, 370, 194  
 Irwin M., Hatzidimitriou D., 1995, *MNRAS*, 277, 1354  
 Jing Y. P., Suto Y., 2000, *ApJ*, 529, L69  
 Kaplinghat M., Knox L., Turner M. S., 2000, *Phys. Rev. Lett.*, 85, 3335  
 Klessen R. S., Kroupa P., 1998, *ApJ*, 498, 143  
 Kleyna J. T., Wilkinson M. I., Evans N. W., Gilmore G., 2001, *ApJL*, 563, 115  
 Kleyna J. T., Wilkinson M. I., Evans N. W., Gilmore G., 2002, *MNRAS*, 330, 792  
 Kroupa P., 1997, *NewA*, 2, 139  
 Lacey C., Cole S., 1993, *MNRAS*, 262, 627  
 Lake G., 1989, *ApJ*, 345, L17  
 Lima Neto G. B., Gerbal D., Márquez I., 1999, *MNRAS*, 309, 481  
 Lokas E. L., 2000, *MNRAS*, 311, 423  
 Lokas E. L., 2001, *MNRAS*, 327, 21P  
 Lokas E. L., Hoffman Y., 2000, *ApJ*, 542, L139  
 Lokas E. L., Hoffman Y., 2001a, in Spooner N. J. C., Kudryavtsev V., eds, *Proc. 3rd International Workshop, The Identification of Dark Matter*. World Scientific, Singapore, p. 121  
 Lokas E. L., Hoffman Y., 2001b, submitted to *MNRAS*, *astro-ph/0108283*  
 Lokas E. L., Mamon G. A., 2001, *MNRAS*, 321, 155  
 Majewski S. R., Ostheimer J. C., Patterson R. J., Kunkel W. E., Johnston K. V., Geisler D., 2000, *AJ*, 119, 760  
 Martínez-Delgado D., Alonso-García J., Aparicio A., Gómez-Flechoso M. A., 2001, *ApJ*, 549, L63  
 Mateo M., 1997, in Arnaboldi M. et al., eds, *ASP Conf. Ser. Vol. 116, The Nature of Elliptical Galaxies*. Astron. Soc. Pac., San Francisco, p. 259  
 Mateo M., 1998a, in Richtler T., Braun J. M., eds, *Proc. Bonn/Bochum-Graduiertenkolleg Workshop, The Magellanic Clouds and Other Dwarf Galaxies*. Shaker Verlag, Aachen, p. 53  
 Mateo M., 1998b, *ARA&A*, 36, 435  
 Mateo M., Olszewski E. W., Welch D. L., Fischer P., Kunkel W., 1991, *AJ*, 102, 914  
 McGaugh S. S., de Blok W. J. G., 1998, *ApJ*, 499, 66  
 Merrifield M. R., Kent S. M., 1990, *AJ*, 99, 1548  
 Merritt D., 1985, *AJ*, 90, 1027  
 Merritt D., 1987, *ApJ*, 313, 121  
 Milgrom M., 1983, *ApJ*, 270, 365  
 Milgrom M., 1995, *ApJ*, 455, 439  
 Moore B., 1994, *Nature*, 370, 629  
 Moore B., Governato F., Quinn T., Stadel J., Lake G., 1998, *ApJ*, 499, L5  
 Navarro J. F., Frenk C. S., White S. D. M., 1997, *ApJ*, 490, 493  
 Oh K. S., Lin D. N. C., Aarseth S. J., 1995, *ApJ*, 442, 142  
 Olszewski E. W., Pryor C., Armandroff T. E., 1996, *AJ*, 111, 750  
 Osipkov L. P., 1979, *PAZh*, 5, 77  
 Piatek S., Pryor C., 1995, *AJ*, 109, 1071  
 Piatek S., Pryor C., Armandroff T. E., Olszewski E. W. 2002, *AJ*, in press, *astro-ph/0201297*  
 Ravindranath S., Ho L. C., Filippenko A. V. 2001, *ApJ*, in press, *astro-ph/0110441*  
 Richstone D. O., Tremaine S., 1984, *ApJ*, 286, 27  
 Salucci P., Burkert A., 2000, *ApJ*, 537, L9  
 Sanders R. H., Verheijen M. A. W., 1998, *ApJ*, 503, 97  
 Sérsic J. L., 1968, *Atlas de Galaxies Australes*, Observatorio Astronomico, Cordoba  
 Thomas P. A. et al., 1998, *MNRAS*, 296, 1061

- Tyson J. A., Kochanski G. P., dell'Antonio I. P., 1998, *ApJL*, 498, 107
- van den Bosch F. C., Swaters R. A., 2001, *MNRAS*, 325, 1017
- van der Marel R. P., Magorrian J., Carlberg R. G., Yee H. K. C., Ellingson E., 2000, *AJ*, 119, 2038
- White S. D. M., Zaritsky D., 1992, *ApJ*, 394, 1
- Wilkinson M. I., Kleyna J. T., Evans N. W., Gilmore G., 2002, *MNRAS*, 330, 778
- Williams L. L. R., Navarro J. F., Bartelmann M., 1999, *ApJ*, 527, 535